Solution Structure of the Cytoplasmic Domain of Erythrocyte Membrane Band 3 Determined by Site-Directed Spin Labeling†

Zheng Zhou,‡ Susan C. DeSensi,§ Richard A. Stein,‡ Suzanne Brandon,‡ Mrinalini Dixit,‡ Erin J. McArdle,‡ Eric M. Warren,§ Heather K. Kroh,‡ Likai Song,|| Charles E. Cobb,‡ Eric J. Hustedt,‡ and Albert H. Beth*,‡

Molecular Physiology and Biophysics and Center for Structural Biology, Vanderbilt University, Nashville, Tennessee 37232, and Institute of Molecular Biophysics, The National High Magnetic Field Laboratory, Department of Biological Sciences, Florida State University, Tallahassee, Florida 32310

Received May 19, 2005; Revised Manuscript Received September 7, 2005

ABSTRACT: The cytoplasmic domain of the anion exchange protein (cdb3) serves as a critical organizing center for protein−protein interactions that stabilize the erythrocyte membrane. The structure of the central core of cdb3, determined by X-ray crystallography from crystals grown at pH 4.8, revealed a compact dimer for residues 55−356 and unresolved N- and C-termini on each monomer [Zhang et al. (2000) *Blood 96*, 2925−2933]. Given that previous studies had suggested a highly asymmetric structure for cdb3 and that pH dependent structural transitions of cdb3 have been reported, the structure of cdb3 in solution at neutral pH was investigated via site-directed spin labeling in combination with conventional electron paramagnetic resonance (EPR) and double electron electron resonance (DEER) spectroscopies. These studies show that the structure of the central compact dimer (residues 55−356) is indistinguishable from the crystal structure determined at pH 4.8. N-Terminal residues 1−54 and C-terminal residues 357−379 are dynamically disordered and show no indications of stable secondary structure. These results establish a structural model for cdb3 in solution at neutral pH which represents an important next step in characterizing structural details of the protein−protein interactions that stabilize the erythrocyte membrane.

The erythrocyte membrane, though similar to other mammalian cellular plasma membranes in terms of total lipid and protein composition, is remarkable in terms of its mechanical stability, deformability, and viscoelastic properties. Extensive biochemical and ultrastructural characterization of the erythrocyte membrane over the past three decades has led to definition of the proteins, and the interactions between these proteins, that stabilize the membrane. In brief, there is an extensive membrane skeleton, composed primarily of the proteins spectrin and actin, that lines the cytoplasmic surface of the membrane. The hexagonal spectrin lattice interacts with the membrane bilayer via two major types of contacts, one involving short actin protofilaments and protein 4.1 interacting with the cytoplasmic domain of glycophorin C, and the second involving the bridging protein ankyrin, protein 4.1, and protein 4.2 interacting with the cytoplasmic domain of anion exchange protein 1 (AE1),[1] also known as band 3 (reviewed in ref *1*).

AE1 is an abundant intrinsic membrane protein in the human erythrocyte comprising approximately 25% of the total membrane protein. It can be cleaved into two structurally and functionally independent domains, each of which maintains their separate functions. The "55 kDa" transmembrane domain (actual molecular weight 59.3 kDa) traverses the bilayer 12 to 14 times thereby forming an anion exchange pathway for chloride and bicarbonate (*2*). The "41 kDa" cytoplasmic domain of band 3 (cdb3; actual molecular weight 42.5 kDa) serves as an important organizing center for a large number of protein−protein interactions (*1*, *3*) including ankyrin (*4*), protein 4.2 (*5*), protein 4.1 (*6*), glycolytic enzymes (*7*−*10*), hemoglobin (*11*−*13*), hemichromes (*14*), and $p72^{syk}$ (*15*). A number of studies carried out over the past two decades have suggested that cdb3 exhibits an elongated, highly asymmetric structure when separated from the transmembrane domain of AE1 as a water soluble protein (*16*, *17*) as well as when present in full length AE1 in the erythrocyte membrane (*18*). The prevailing model of cdb3 throughout the 1980s and 1990s was that the cdb3 dimer folded into a rodlike domain that extended into the cytosolic compartment of the erythrocyte with the N-terminus far from the cytoplasmic surface of the membrane. Consequently, it was a major surprise when the X-ray crystal structure of cdb3 (residues 1−379) showed a compact symmetric dimer

† This work was supported by Grant R37 HL034737 (A.H.B.) from the National Institutes of Health. The EPR instrumentation at the National High Magnetic Field Laboratory was purchased on Grant CHE-0079649 from the National Science Foundation, and predoctoral support was provided by the American Heart Association (L.S.).

* Corresponding author: Tel: 615-322-4235. Fax: 615-322-7236. E-mail: al.beth@vanderbilt.edu.

‡ Molecular Physiology and Biophysics, Vanderbilt University.

§ Center for Structural Biology, Vanderbilt University.

|| Florida State University.

[1] Abbreviations: AE1, anion exchanger 1; CD, circular dichroism; cdb3, cytoplasmic domain of band 3; CW, continuous wave; DEER, double electron electron resonance; DQC, double quantum coherence; DSC, differential scanning calorimetry; EPR, electron paramagnetic resonance; MTSSL, 1-oxyl-2,2,5,5-tetramethyl-Δ3-pyrroline-3-methyl methanethiosulfonate spin label; NiEDDA, nickel(II) ethylenediaminediacetate; PBS, phosphate buffered saline; SDSL, site-directed spin labeling; SDS−PAGE, sodium dodecyl sulfate polyacrylamide gel electrophoresis; TPX, trademark for polymethylpentene.

10.1021/bi050931t CCC: $30.25
Published on Web 10/29/2005

stabilized by interlocking dimerization arms and with each subunit exhibiting a large peripheral domain with an α^+ β-fold (*3*). Equally as surprising, the unresolved N- and C-termini did not exit the dimer on opposite surfaces, a geometry that would seem reasonable for optimal exposure of the N-terminus for binding to intracellular proteins (*3*).

Given that cdb3 was crystallized at the nonphysiological pH of 4.8 and that several studies have indicated that cdb3 undergoes two reversible conformational rearrangements as a function of pH with midpoints at 7.2 and 9.2 as reported by intrinsic tryptophan fluorescence (e.g. ref *19*), it is possible that the structure of cdb3 determined at pH 4.8 does not accurately reflect the structure at physiological pH and, by extension, the structure of this domain in the intact erythrocyte. To address the question of how the structure of cdb3 at neutral pH compares with the crystal structure determined at pH 4.8, we have carried out a series of site-directed spin-labeling experiments on cdb3. These studies have shown that the structure of the central compact region of the cdb3 dimer (residues 55−356) at neutral pH is indistinguishable from the crystal structure reported at pH 4.8 (*3*). In addition, these studies have shown that the N-terminus (residues 1−54), which was not resolved in the crystal structure, is dynamically disordered with no indications of regions of stable secondary structure. Likewise, the C-terminus (residues 357−379) is also dynamically disordered, suggesting a very flexible linkage between the compact central region of cdb3 and the transmembrane domain of AE1. Portions of this work have appeared as abstracts (*20*−*22*).

MATERIALS AND METHODS

Cloning and Site-Directed Mutagenesis. The full length human AE1 DNA was kindly provided by Dr. Robert Gunn (Emory University). The segment of the cDNA encoding residues 1−379 of AE1 was amplified using Pfu DNA polymerase (Stratagene, La Jolla, CA) with the N-terminal (forward) primer ACGGGAATTCCATATGGAGGAGCTGCAGGATGATTATG and the C-terminal (reverse) primer TCACACCGCTCGAGTTATTAGAAGAGCTGGCCTGTCTGCTG (IDT DNA, Coraville, IA). The PCR product was cloned into the pET-19b vector (Novagen, Madison, WI) between the *Nde*I and *Xho*I sites and designated as pZZ3_WT. The cysteineless mutant and single cysteine mutants were constructed by using the QuikChange Site-Directed Mutagenesis Kit (Stratagene, La Jolla, CA). The sequences of all mutants were confirmed by DNA sequencing.

Protein Preparation. pZZ3 plasmids were transformed into BL21 Gold (DE3) *Escherichia coli* competent cells (Stratagene, La Jolla, CA). Expression of cdb3 was followed by the autoinduction protocol developed by Dr. F. William Studier (Brookhaven National Laboratory) (*23*). Briefly, overnight starter cultures were grown in PAG at 37 °C and 200 μL of the starter cultures was used to inoculate 200 mL of ZYP-5052 for overnight autoinduction (14 h). Typically, saturation (A_{600} = 4.8−7.0) was reached in about 10 h at 37 °C. Additional incubation for 4 h maximized lactose autoinduction. His-tagged cdb3 purification was carried out using Ni-NTA resin as described by the manufacturer (Qiagen, Valencia, CA). For some mutants, the N-terminal His tag was cleaved via the Enterokinase Cleavage Capture Kit (Novagen, Madison, WI). For certain mutants, gel filtration was performed on an HPLC TSK G3000SW column (Toso-Haas, Montgomeryville, PA). Protein concentration was determined by UV absorption at 280 nm using an extinction coefficient of 33 000 M^{-1} cm^{-1}. Purity of the expressed proteins was at least 95%, as determined by SDS−PAGE (*24*). Single cysteine mutants were spin-labeled with a 10-fold molar excess of 1-oxyl-2,2,5,5-tetramethyl-Δ3-pyrroline-3-methyl methanethiosulfonate spin label (MTSSL; Toronto Research Chemicals, North York, ON, Canada) in the dark at room temperature for 2 h and then at 4 °C overnight in a buffer containing 50 mM NaH_2PO_4, 300 mM NaCl, and 200 mM imidazole, pH 8.0. To singly spin label the cdb3 dimer, MTSSL and a non-paramagnetic label (1-acetyl-2,2,5,5-tetramethyl-Δ3-pyrroline-3-methyl methanethiosulfonate; Toronto Research Chemicals, North York, ON Canada) were used at a 1:5 molar ratio. Unreacted label was removed from all samples by reconcentrating 4 times (1:50 v/v) in an Amicon Ultra-4 centrifugal filter device (30 kDa nominal molecular weight limit, Millipore, Bedford, MA) with a buffer containing 20 mM NaH_2PO_4, 100 mM NaCl, 1 mM EDTA, pH 6.8. All EPR and DEER measurements reported were collected with the spin-labeled samples in this buffer at pH 6.8. Identical spectral results were obtained on samples recorded in this same buffer at pH 8.0 (data not shown). The disulfide bond between the spin label and the cysteine side chain is more stable at the lower pH thereby facilitating the storage and shipping of samples for recording DEER data at the National High Magnetic Field Laboratory.

Circular Dichroism and Differential Scanning Calorimetry. CD spectra were recorded on a Jasco J-810 system (Easton, MD) at room temperature in a 0.1 cm path length cell. All spectra were obtained in buffer containing 10 mM NaH_2PO_4, 1 mM EDTA, pH 7.4. The data were collected from 190 to 260 nm at a scan speed of 10 nm/min. The raw data, in millidegrees (θ), were converted to molar ellipticity [θ] using the relationship

$$[\theta] = (100\theta)/(ncl)$$

where n is the number of amino acid residues, c is the protein concentration in mM, and l is the path length in cm.

DSC measurements were carried out on a MicroCalorimetry VP-DSC instrument (Northampton, MA) at a protein concentration of 1−2 mg/mL. The samples were prepared in 10 mM NaH_2PO_4, 1 mM EDTA, pH 7.4. The sample and buffer were degassed for 5 min at 20 °C before being loaded into the tantalum sample cell and reference cell, respectively. The data were collected in the range of 20−100 °C at a scan rate of 1.5 °C/min.

CW-EPR Measurements. X-band (9.8 GHz) CW-EPR spectra were collected using a Bruker EMX spectrometer equipped with a TM_{110} cavity (BrukerBiospin, Billerica, MA) at room temperature. Samples prepared at 100 μM spin concentration were drawn into 50 μL glass capillaries (VWR, West Chester, PA) and sealed with Critoseal sealant (Fisher, Pittsburgh, PA). Samples for distance measurements by CW-EPR spectroscopy were prepared in 50% sucrose (w/w) and controlled at 2 °C by a standard Bruker variable-temperature unit. CW-EPR spectra were acquired at 5 mW microwave power using 100 G sweep widths. All spectra contain 1024 data points collected at a 100 kHz Zeeman field modulation frequency of 1.25 G amplitude (peak-to-peak) and a 42 s

sweep time. The second moment, $\langle\omega^2\rangle = \int\omega^2 f(\omega)\, d\omega / \int f(\omega)\, d\omega$, was calculated as a measure of the breadth of the EPR spectra (*25*). Distances between spin-labeled sites in some samples were determined from fitting of CW-EPR spectra either using a tether-in-a-cone model (*26*) or by spectral convolution assuming a Gaussian distance distribution (*27, 28*) as defined in the table and figure legends.

Solvent Accessibility. Solvent accessibility of individual spin-labeled residues was measured on samples diluted to 100 μM spin concentration in 20 mM NaH_2PO_4, 100 mM NaCl, 1 mM EDTA, pH 6.8. NiEDDA was added at a concentration of 1 mM. Samples were purged of molecular oxygen by flowing nitrogen gas over the sample contained in a TPX capillary for 15 min prior to and during measurements. A 25 G scan of the central resonance line for each mutant was carried out using a 1 G modulation amplitude of 100 kHz frequency. A total of 24 scans were separately recorded at microwave powers ranging from 1 mW to 200 mW (1 dB attenuation/step). Data were analyzed by nonlinear least squares curve fitting using Origin 6.1 software (OriginLab Corporation, Northampton, MA) of the spectral amplitude (A_0) versus the square root of microwave power ($\sqrt{P_0}$) using the equation

$$A_0 = \frac{c\Lambda\sqrt{P_0}}{[1 + (2^{1/\epsilon} - 1)P_0/P_{1/2}]^{\epsilon}} + N_0$$

where A_0 is the peak-to-peak amplitude of the first derivative spectrum, c is the instrumental proportionality constant, Λ is the instrumental factor, P_0 is the input power, ϵ is the line shape adjustment parameter, $P_{1/2}$ is the half-saturation power, and N_0 is the noise correction factor. The NiEDDA accessibility is calculated by the following equation:

$$\mathrm{Ac(NiEDDA)} = \frac{P_{1/2}(\mathrm{NiEDDA}) - P_{1/2}(\mathrm{N_2})}{\Delta H_0}$$

where Ac is the accessibility, $P_{1/2}$ (NiEDDA) is the half-saturation power in the presence of 1 mM NiEDDA, $P_{1/2}$ (N_2) is the half saturation power in the absence of NiEDDA, and ΔH_0 is the central line width (*29, 30*).

DEER Measurements. Long-range nitroxide−nitroxide distances were measured by double electron electron resonance (DEER) spectroscopy. DEER experiments were performed at X-band using a Bruker E680 X/W-band pulsed EPR instrument (Bruker Spectrospin, Billerica, MA) at the National High Magnetic Field Laboratory (Tallahassee, FL) using a 4-pulse sequence (*31*). For DEER measurements, spin-labeled cdb3 dimer samples were approximately 300 μM in spin label concentration as measured by the doubly integrated intensity of the room temperature CW-EPR spectrum in comparison to a standard of known spin concentration. All samples contained 30% (w/w) glycerol. All DEER experiments were performed at 65 K using a 1 ms shot repetition time and a 16 ns 90° pulse width in an overcoupled dielectric resonator (ER 4118X-MD5, Bruker Biospin, Billerica, MA). The 180° ELDOR pulse was 32 ns wide at 70 MHz frequency offset. DEER data were analyzed using the DeerPackage 2002.1 software made available by G. Jeschke (Max Planck Institute for Polymer Research, Mainz, Germany (*32*−*34*)) assuming a single Gaussian distance distribution.

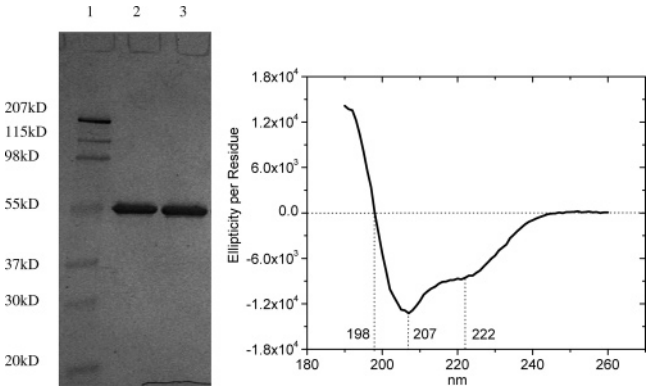

FIGURE 1: SDS−PAGE and circular dichroism of cdb3. The left panel shows the SDS−PAGE of molecular weight standards (lane 1), wt-cdb3 (lane 2), and cysless-cdb3 (lane 3). The right panel shows the CD spectrum (190−260 nm) of recombinant wt-cdb3.

Intrinsic Tryptophan Fluorescence. Purified cysless-cdb3 and wt-cdb3 were concentrated and buffered-exchanged into a pH 7.0 phosphate−borate buffer (50 mM sodium phosphate, 50 mM boric acid, 70 mM NaCl, 2 mM EDTA). Tryptophan fluorescence emission spectra were collected on 150 μL samples of wt-cdb3 and cysless-cdb3 diluted to a final concentration of 50 μg/mL (5 mg/mL stock solutions, diluted 100× in buffer of the desired pH). Identical experimental results were also obtained on samples in a phosphate−citrate buffer over the same pH range (20 mM sodium phosphate, 20 mM citric acid, 2mM EDTA; data not shown). The emission spectra were collected on a PTI Quantamaster 2000-7SE fluorometer (Photon Technology International, Lawrenceville, NJ) at room temperature, using an excitation wavelength of 290 nm and collecting fluorescence emission from 300 to 400 nm (both excitation and emission slit widths were set at 2 nm). Data are presented as the center of mass wavelength of the emission spectra (i.e., the spectral midpoint wavelength where half of the total emission is above and half is below).

Molecular Modeling. Molecular models of the spin-labeled cdb3 mutants were manually constructed from the known crystal structure of cdb3 (PDB ID: 1HYN (*3*)) using the molecular graphics program PSSHOW. Estimates of the distance between spin labels were obtained using the $\chi_4\chi_5$ model (Figure 3 (*35, 36*)). The torsion angles of the first three bonds between C_α of the spin-labeled cysteine and the nitroxide ring were fixed to $\chi_1 = -60°$, $\chi_2 = -60°$, and $\chi_3 = -90°$, respectively, while χ_4 and χ_5 were iteratively rotated in steps of 30° within NAB (*37*). After each rotation, the distance between the spin labels was measured from points equidistant between the nitrogen and oxygen atoms of the nitroxides. The distance was rejected if the orientation of the spin label resulted in overlap with any other atom in the structure greater than 0.4 times the sum of the van der Waals radii. The average and standard deviation of the accepted distances were then computed.

RESULTS

Characterization of Recombinant Cdb3. Recombinant wt-cdb3, cysless-cdb3, and all single cysteine mutants of cdb3 in the cysless background were expressed and purified

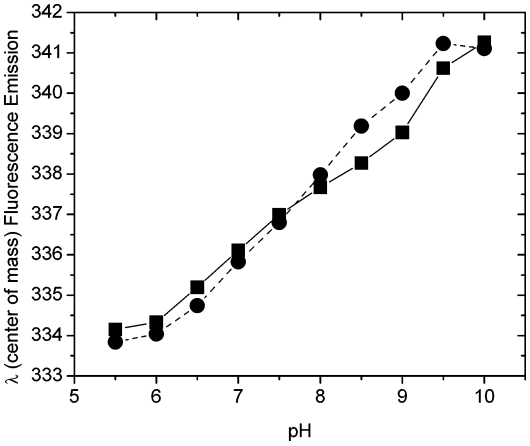

FIGURE 2: Intrinsic tryptophan fluorescence. The filled squares are from wt-cdb3, and the filled circles are from cysless-cdb3. The data are plotted as the wavelength (λ) at the center of mass of the tryptophan fluorescence emission spectrum versus pH. All data were collected as described in Materials and Methods.

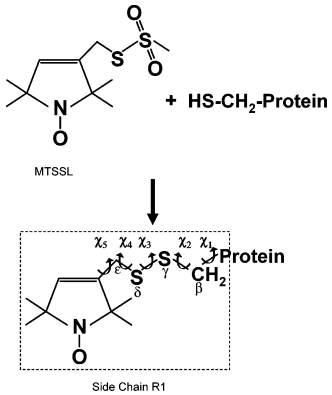

FIGURE 3: Protein labeling with MTSSL. The reaction of cysteine with MTSSL yields the spin-labeled side chain denoted R1. The dihedral angles χ_1 through χ_5, which relate the spin label moiety to the backbone C_α carbon, are defined in accordance with the previous literature (*35*).

as described in Materials and Methods. The purity of cdb3 was greater than 95% as determined by SDS−PAGE for all samples used in this work (Figure 1). A single dominant band was observed in native gel electrophoresis, and a single peak eluted from size exclusion chromatography, suggesting that recombinant cdb3 adopts a single conformation (data not shown). The position of the eluted peak, in comparison with molecular weight standards, confirmed that recombinant wt-cdb3 and all mutants examined exist as dimers in solution at neutral pH. More evidence of a dimeric structure will be discussed in the following sections. Circular dichroism (CD) was employed to evaluate the secondary structure of recombinant cdb3. The CD spectrum from recombinant wt-cdb3 (Figure 1) exhibited a crossover point near 198 nm, a negative extremum at 207 nm, and a shoulder at 222 nm and was indistinguishable from the CD spectrum reported for cdb3 isolated from human erythrocytes (*16*). The melting temperature (T_m) of wt-cdb3, as monitored by differential scanning calorimetry (DSC), was 70 °C at pH 7.4 (data not shown), close to the value of 68 °C reported previously for erythrocyte cdb3 (*16*). Collectively, these data indicate that the construct of wt-cdb3 containing a His_9 tag at the N-terminus that was expressed and purified from *E. coli* exhibited essentially the same secondary and quaternary structure and essentially the same thermal stability as wt-cdb3 that was isolated from the erythrocyte membrane. The EPR data obtained from His_9-cdb3 was indistinguishable from the data obtained following cleavage of the His_9 tag from the N-terminus (data not shown). Therefore, all spectra presented were obtained from His_9-cdb3.

Intrinsic Tryptophan Fluorescence in Recombinant Wt-cdb3 and Cysless-cdb3. Previous work has shown that wt-cdb3 undergoes two fully reversible pH-dependent conformational changes in the range from 6 to 10 (*16*, *19*, *38*, *39*). These studies have provided strong evidence that cdb3 can exist in three different conformations with the midpoints for the transitions at pH 7.2 and 9.2, that the transitions do not involve changes in the secondary structure of cdb3, and that there is an increase in molecular asymmetry and segmental dynamics as the pH is increased (*19*, *38*, *39*). Previous work (*19*) has shown that recombinant cdb3 (residues 1−379) undergoes the same conformational transitions as cdb3 isolated from erythrocyte membranes. However, other work indicated that chemical modification or cross-linking of the two endogenous cysteine residues of wt-cdb3 led to a merging of the two structural transitions into a single transition with a midpoint at pH 8.7 (*38*). Since one of the main goals of the current work was to compare the solution structure of cdb3 at neutral pH with the crystal structure determined at pH 4.8, and since the two endogenous cysteines were mutated to alanines prior to introduction of a single cysteine at a selected position for site-directed spin labeling, it was important to compare the magnitude of the change in tryptophan fluorescence in recombinant wt-cdb3 with recombinant cysless-cdb3. As shown in Figure 2, very comparable changes in tryptophan fluorescence were observed as a function of pH indicating that very similar conformational changes were occurring in both proteins.

Structure and Packing of Residues 127−137 in the Peripheral Domain of Cdb3. Residues 127 to 137 form an α-helix in the crystal structure at pH 4.8 with one surface of the helix packed against the central β-sheet and the opposite surface exposed to solvent. To assess whether this structural feature was preserved at neutral pH, each residue from 127 to 137 was mutated to cysteine, one at a time. The proteins were expressed, purified, and spin labeled with MTSSL to yield the spin-labeled side chain denoted R1 (Figure 3). The EPR spectrum at each position is shown in Figure 4. Solvent accessibility was measured for each of these spin-labeled proteins using NiEDDA as a water soluble paramagnetic broadening agent (*40*, *41*) as shown in Figure 5. These data show a sinusoidal change in accessibility to NiEDDA with a period of approximately 3.6 residues characteristic of an α-helix with one surface exposed to solvent and the opposite surface buried in a structured region of the protein. Residues 128, 131, 132, and 135 are the least accessible to the aqueous paramagnetic broadening agent in complete agreement with the packing of the same surface of this α-helix against the β-sheet as determined in the crystal structure (Figure 4). The rotational mobility of the spin-labeled side chains at each of these buried positions was also hindered relative to the adjacent surface exposed sites on the opposite face of the helix as shown in Figure 5 by the inverse second moment of the EPR spectrum (*41*). Together, these results provide strong evidence that the structure of this surface helix, and by inference, the surrounding protein

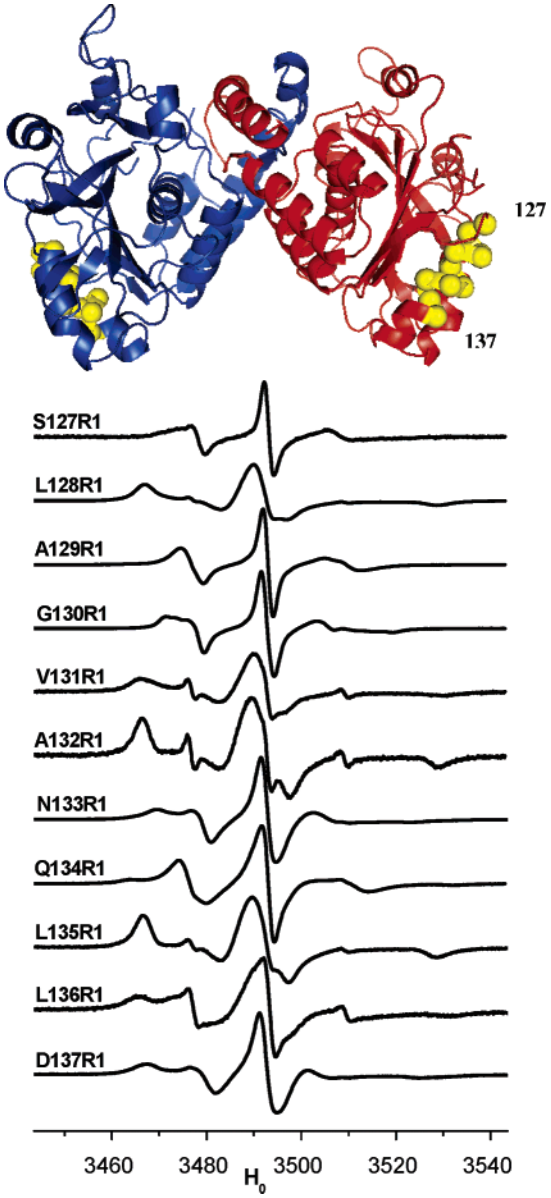

FIGURE 4: EPR characterization of residues 127−137. The upper panel shows the structure and location of residues 127−137 in the crystal structure (yellow) on the ribbon diagram of the two subunits of the cdb3 dimer (blue and red). The conventional CW-EPR spectrum at each position is shown in the lower panel normalized to the same amplitude and with a total scan width of 100 G.

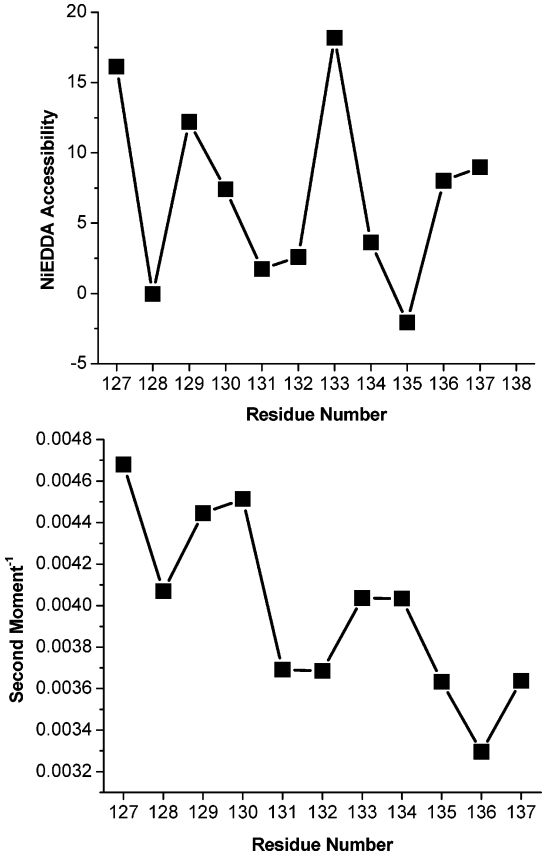

FIGURE 5: Parametrized data from residues 127−137. The upper panel shows a plot of the accessibility of the R1 side chain at each indicated residue to NiEDDA. The lower panel shows a plot of the inverse second moment of the conventional CW-EPR spectrum (Figure 4) at each residue. The parameters were calculated from the EPR data as described in Materials and Methods.

structure in the peripheral domain of cdb3, is the same in solution at neutral pH as it is in the crystal lattice at pH 4.8.

Structure of the Dimer Interface in Cdb3. The high stability of the cdb3 dimer can be explained by the extensive interactions between the "dimerization arms" of each monomer observed in the crystal structure (*3*). The dimerization arms of each monomer (residues 314−344) are composed of helix $\alpha 9^{304-316}$, β strand $\beta 11^{318-323}$, and helix $\alpha 10^{328-347}$. The close packing of residues of cdb3 around helix 9 and β strand 11 in the crystal structure suggested that these regions might be difficult to characterize by site-directed spin labeling given the lack of contrast (i.e. limited solvent exposure) and potential difficulty in stoichiometric spin labeling of introduced cysteine residues in these secondary structure elements. However, based on the static structure, helix 10 was predicted to be an attractive and informative segment for SDSL characterization. Hence, the structure and packing of the C-terminal portion of helix 10 (residues 337−348) was investigated as shown by the EPR spectra in Figure 6. Accessibility to NiEDDA showed a periodicity of approximately 3.6 residues with local minima in the accessibility profile at residues 339, 342, 345, and 346 as shown in Figure 7. The accessibility data are in close agreement with side-chain mobility measurements which showed local minima at residues 339, 342, and 346 as revealed by the inverse second moment of the EPR spectrum (Figure 7). The data in Figure 7 also suggest that there is a monotonic increase in average accessibility and side-chain mobility in progressing from residue 337 to 348. These findings are all consistent with residues 337 to 348 forming an α-helix with greater solvent exposure at the C-terminal end and with the same face of the helix packed in the interior of the cdb3 dimer, as predicted by the crystal structure determined at pH 4.8 (*3*).

The EPR spectrum observed with the R1 side chain at residue 339 gives a highly resolved dipolar coupling between the spin labels on each monomer. The magnitude of this intersubunit dipolar coupling provides a direct measure of the distance between these two spin-labeled side chains in the cdb3 dimer (*26*, *27*, *42*−*44*). The data in Figure 8 show the spectral effects of the intersubunit dipolar coupling (compare the double labeled and the single labeled samples). Analysis of the double labeled spectrum using a tether-in-a-cone model (*26*) yielded an interprobe distance of 14.7 Å. As discussed more fully below, this distance is very close

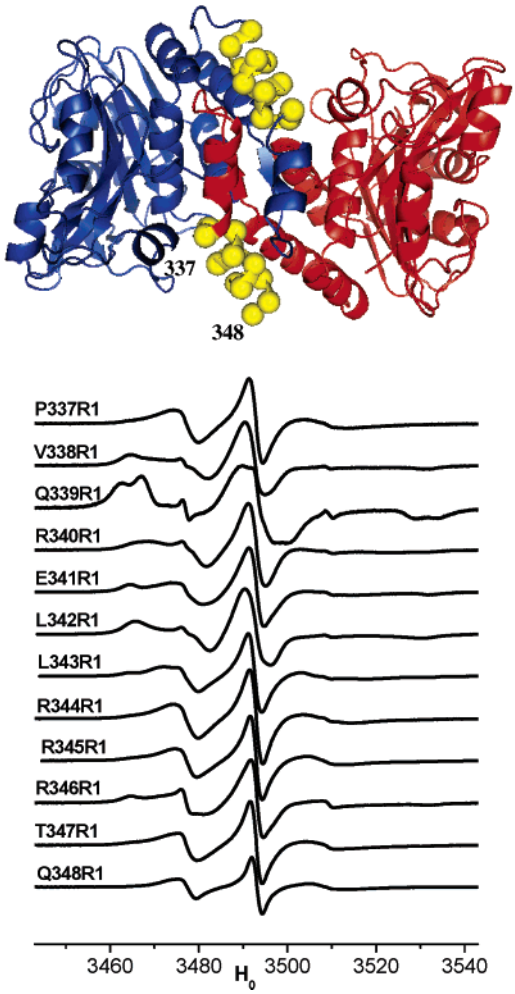

FIGURE 6: EPR characterization of residues 337−348. The upper panel shows the structure and location of residues 337−348 in the crystal structure (yellow) on the ribbon diagram of the two subunits of the cdb3 dimer (blue and red). The conventional CW-EPR spectrum at each position is shown in the lower panel normalized to the same amplitude and with a total scan width of 100 G.

to the distance predicted from the static crystal structure with a spin-labeled cysteine residue modeled at position 339 in place of the normal wild-type glutamine residue.

Intersubunit Distances between Residues 340−345 of the Dimerization Arm. To more fully characterize the spatial arrangements of the dimerization arms of the two monomers in the cdb3 dimer, pulsed double electron electron resonance (DEER) measurements were carried out with spin-labeled cysteine residues in positions 340 through 345. Representative data are shown in Figure 9. DEER is a pulsed EPR technique that extends the maximum interprobe distance that can be measured from the 20 to 25 Å range by CW-EPR methods (*27*, *42*−*44*) out to the 40 to 50 Å range (reviewed in ref *45*). The sensitivity to long distances permits placing spin label probes at sequential positions that are not likely to disrupt the structure of the dimer interface due to changes in packing of side chains in the interior of the protein while still providing direct information on the spatial arrangement of the dimerization arms. The data in Figure 10 show that the interprobe distances measured from CW-EPR (residue 339; Figure 8) and DEER (residues 340−345; Figure 9; data from all sites compiled in Table 1) experiments followed the same trend as the $C_\alpha-C_\alpha$ distances measured from the corresponding residues in the crystal structure at pH 4.8.

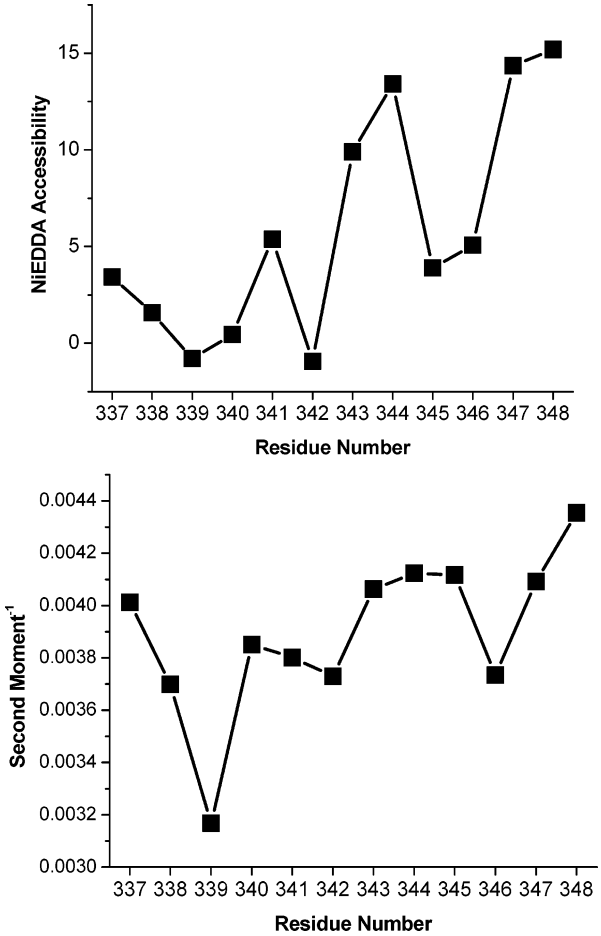

FIGURE 7: Parametrized data from residues 337−348. The upper panel shows a plot of the accessibility of the R1 side chain at each indicated residue to NiEDDA. The lower panel shows a plot of the inverse second moment of the conventional CW-EPR spectrum (Figure 6) at each residue. The parameters were calculated from the EPR data as described in Materials and Methods. At residue 339, the second moment was calculated from the EPR spectrum obtained after single labeling (see Figure 8, lower) thereby avoiding including the contributions of dipolar coupling.

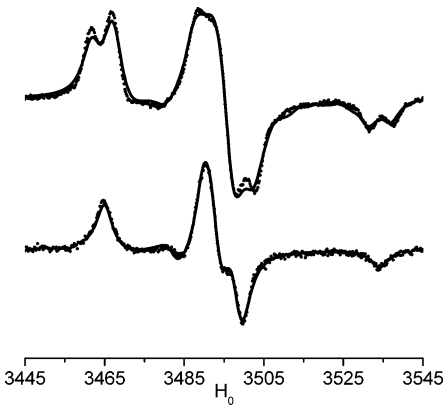

FIGURE 8: Analysis of EPR data at residue 339. The experimental EPR spectra under conditions of double labeling (R1 side chain incorporated in both subunits; upper) and single labeling (R1 side chain in only a fraction of sites in one subunit; lower) are shown as dots. The best-fit computer simulations for each spectrum are shown as solid lines. Analysis of the lower single labeled spectrum (*68*) allowed determination of the principal elements of the **A** and **G** tensors: $g_{xx} = 2.0079$; $g_{yy} = 2.0062$; $g_{zz} = 2.0024$; $A_{xx} = 7.82$ G; $A_{yy} = 2.81$ G; and $A_{zz} = 34.51$ G. These values were used as input parameters for fitting the upper double labeled spectrum (*26*) to determine the interprobe separation (14.7 Å) and the width of the distance distribution (0.4 Å).

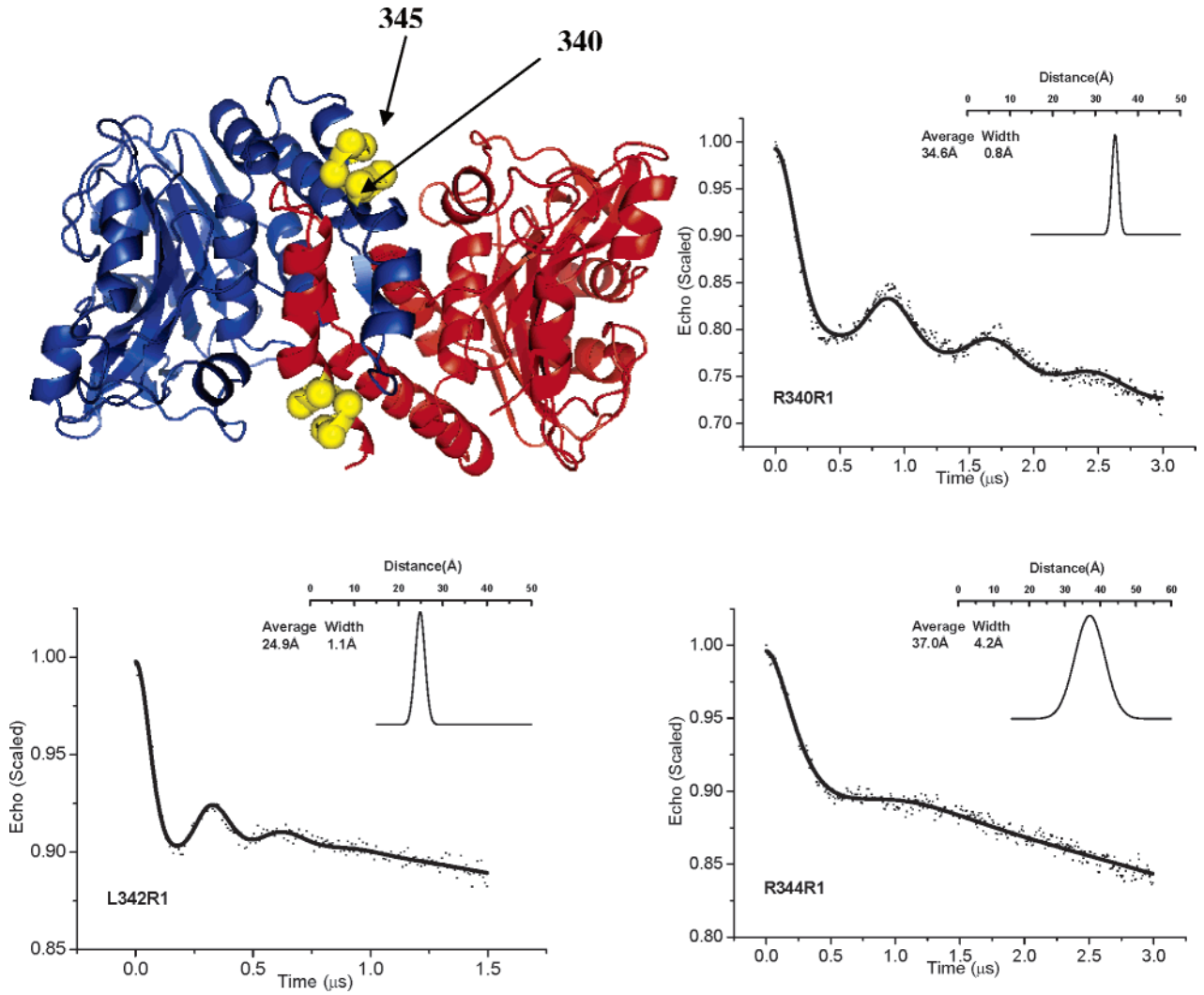

FIGURE 9: DEER characterization of intersubunit distances between residues 340−345 in the dimerization arm. The upper left panel shows the structure and location of residues 340−345 in the crystal structure (yellow) on the ribbon diagram of the two subunits of the cdb3 dimer (blue and red). The scaled echo amplitude (shown as dots, normalized to 1) is plotted as a function of time in a 4-pulse DEER experiment with the R1 side chain at positions 340 (upper right), 342 (lower left), and 344 (lower right). The solid line is the best fit of the scaled echo amplitude versus time using DeerPackage 2002.1 as described in Materials and Methods. The insets in the upper right of each DEER spectrum show the average interprobe distance and the distribution of distances from fitting the experimental data. Tabular data for residues 341 and 343 (DEER data not shown) are listed in Table 1.

Table 1: Interresidue Distances in the Dimerization Arm of Cdb3

residue no.:	339	340	341	342	343	344	345
R (Å)	14.7[a]	34.6	31.9	24.9	34.0	37.0	35.5
σ (Å)	0.4[a]	0.8	3.6	1.1	2.3	4.2	6.6

[a] The values for R and σ at residue 339 were obtained by fitting the CW-EPR data to a tether-in-a-cone model (*26*). The values for R and σ at positions 340 through 345 were determined by fitting the corresponding DEER data to a single Gaussian distribution of interspin distances as described in Materials and Methods.

Also shown in Figure 10 are the predicted average distances between the unpaired electrons of the two spin labels from molecular modeling of the R1 side chain at each site based on the static crystal structure. The results of these modeling experiments, which were carried out to approximate contributions from the dimensions and flexibility of the R1 side chain as described in Materials and Methods (see refs *46*−*49* for additional discussion), are in reasonable agreement with the interprobe distances that were obtained from the experimental measurements. When combined with the data in Figure 7, which showed that residues 337−348 form a continuous α-helix, these long-range distance constraints show that the spatial arrangement of these two helices in the cdb3 dimer is very similar, if not identical, to their spatial arrangement in the crystal structure at pH 4.8.

Intersubunit Distances at Additional Sites. Previous studies have provided compelling evidence that the Stokes radius of cdb3 reversibly increases from 55 to 66 Å as the pH is raised in the range of 6 to 10 with the most dramatic increase (~80%) occurring between pH 8 and 10 (*3*, *19*, *38*). Based on the crystal structure, it has been hypothesized that cdb3 could form elongated structures without an overall change in secondary structure, by rotations about residues G305 or E291 (*3*). To test whether cdb3 exhibited a significantly elongated structure at neutral pH relative to the static crystal structure, 11 different sites on the side of the compact peripheral domain of each monomer that is proximal to the dimer interface were chosen for measurement of interprobe distances as shown in Figure 11. Following expression, purification, and spin labeling of each of these 11 single cysteine mutants, EPR or DEER experiments were carried

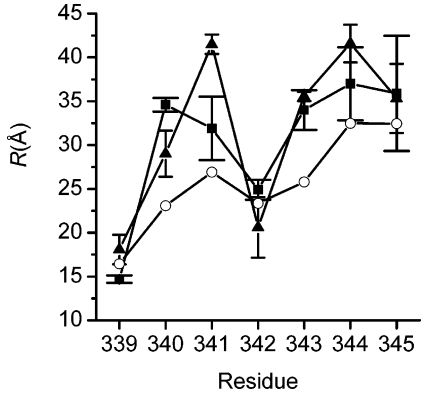

FIGURE 10: Comparison of calculated and experimentally determined interprobe distances in the dimerization arm. The open circles show the $C_\alpha-C_\alpha$ distances from the crystal structure. The filled squares are the experimentally determined inter-R1 distances determined from fitting the CW-EPR data (339) or the DEER data (340−345). The vertical bars are the widths of the distance distributions determined from fitting the experimental data. The filled triangles are the predicted average distances and the widths of the distance distributions that were calculated by modeling the R1 side chain into the crystal structure at each position. The widths of the distance distributions were calculated by positioning the spin label at all allowed orientations (no steric clashes with nearby residues) by rotation about dihedral angles χ_4 and χ_5 (Figure 3).

out and analyzed to determine the average interprobe separation distance and the distribution of interprobe distances (Table 2). Figure 11 demonstrates that the average distances from these measurements agree extremely well with the $C_\alpha-C_\alpha$ distances measured from the crystal structure but do not agree well, either in general trend or in magnitude, with the two elongated models that were generated by rotations about E291 or about G305.

Structure of the N-Terminus of Cdb3. N-Terminal residues 1−54 were not resolved in the crystal structure of cdb3, presumably due to this region of the protein being disordered (either static or dynamic) in the crystal lattice (*3*). Given the central role that the N-terminus plays in binding several intracellular proteins, it is important to determine the structure and dynamics of this region. Toward this goal, single cysteine residues were introduced into cdb3 at positions 2, 15, 16, 34−38, 45, 46, and 48−56 and spin labeled, and the CW-EPR spectra were recorded at each of these positions as shown in Figure 12. At sites 2, 15, 16, 34, 35, 36, 37, 38, 45, and 46 the EPR spectra were indicative of fast, relatively unrestricted motion as would be expected for a dynamically disordered peptide lacking stable secondary structure in solution. From residues 48 to 56 there was a monotonic decrease in mobility until residues 54 through 56, where the EPR spectra were characteristic of a spin-labeled side chain in a structured environment in tertiary contact with nearby elements of secondary structure (*41*). These data, which are consistent with the boundary between structured and disordered domains in the crystal structure, demonstrate that the N-terminus of cdb3 lacks stable secondary structure and exists in solution as a highly flexible and dynamic structure on the nanosecond time scale that is capable of accessing the full range of available conformational states.

Structure of the C-Terminus of Cdb3. The structure of the C-terminus of cdb3 is of considerable interest since this segment forms the physical link with the transmembrane domain of AE1. Previous work has suggested that there is a flexible linkage between the two independent domains of AE1 (*50*) and that this flexibility may be critical for maintenance of the unusual mechanical properties of the erythrocyte membrane (*51*−*53*). Single cysteine residues were introduced at positions 357, 358, 361, 364, 368, 372, 376, and 378 and spin labeled, and the EPR spectra were recorded as shown in Figure 13. At all of these positions, the EPR spectra were indicative of relatively unrestricted motion as would be expected for peptide lacking stable secondary structure in solution.

DISCUSSION

Recent progress in determination of the atomic resolution structures of cdb3 (*3*) and a large fragment of ankyrin (*54*) has enabled the design of new experiments aimed at assembling atomic, or near atomic, resolution models of the complex of proteins that are known to stabilize the erythrocyte membrane. An essential starting point for establishing these models is an accurate knowledge of the solution structure of cdb3 at physiological pH. For many proteins, determination of the atomic resolution structure at a non-physiological pH would be adequate. However, for cdb3, previous hydrodynamic studies (*16*, *17*) had suggested a highly elongated structure that was quite different than the compact globular structure that was determined in the crystal lattice. The hydrodynamic studies, coupled with the knowledge that intrinsic tryptophan fluorescence (e.g. ref *19*), thermal stability (*16*), stokes radius (*38*), and segmental dynamics (*39*) all exhibited significant changes as a function of pH in the range from 6 to 10, provided suggestions that the structure of cdb3 could be significantly different at pH 4.8 than in the physiological 7.2 to 7.4 range.

In addition to raising concerns about the magnitude of structural changes that occur as a function of pH, previous studies had not led to a clear elucidation of the structure and dynamics of the N- and C-terminal segments of cdb3. Neither of these regions was resolved in the crystal structure. However, they both play key roles in the overall function of cdb3 with the N-terminus serving as a critical organizing center for binding to a number of intracellular proteins (reviewed in ref *1*) and the C-terminus forming a physical link to the transmembrane domain of AE1. To address the magnitude of structural changes that occur as a function of pH and to elucidate the structure and dynamics of the N- and C-terminal segments, the two endogenous cysteines in

Table 2: Interresidue Distances between Selected Sites Not at the Dimer Interface

residue no.:	84	96	105	108	112	116	142	199	208	277	290
R (Å)	27.2	32.6	15.4	6.2[a]	18.0[a]	17.4	32.1	36.2	47.7	29.8	38.4
σ (Å)	2.5	5.0	3.7	4.4[a]	6.9[a]	3.1	3.1	5.0	13.2	3.4	0.5

[a] The values for R and σ at positions 108 and 112 were determined by fitting the CW-EPR data with a convolution method assuming a single Gaussian distribution of distances (*27*). The values at all other residues were determined by fitting the corresponding DEER data to a single Gaussian distribution of distances as described in Materials and Methods.

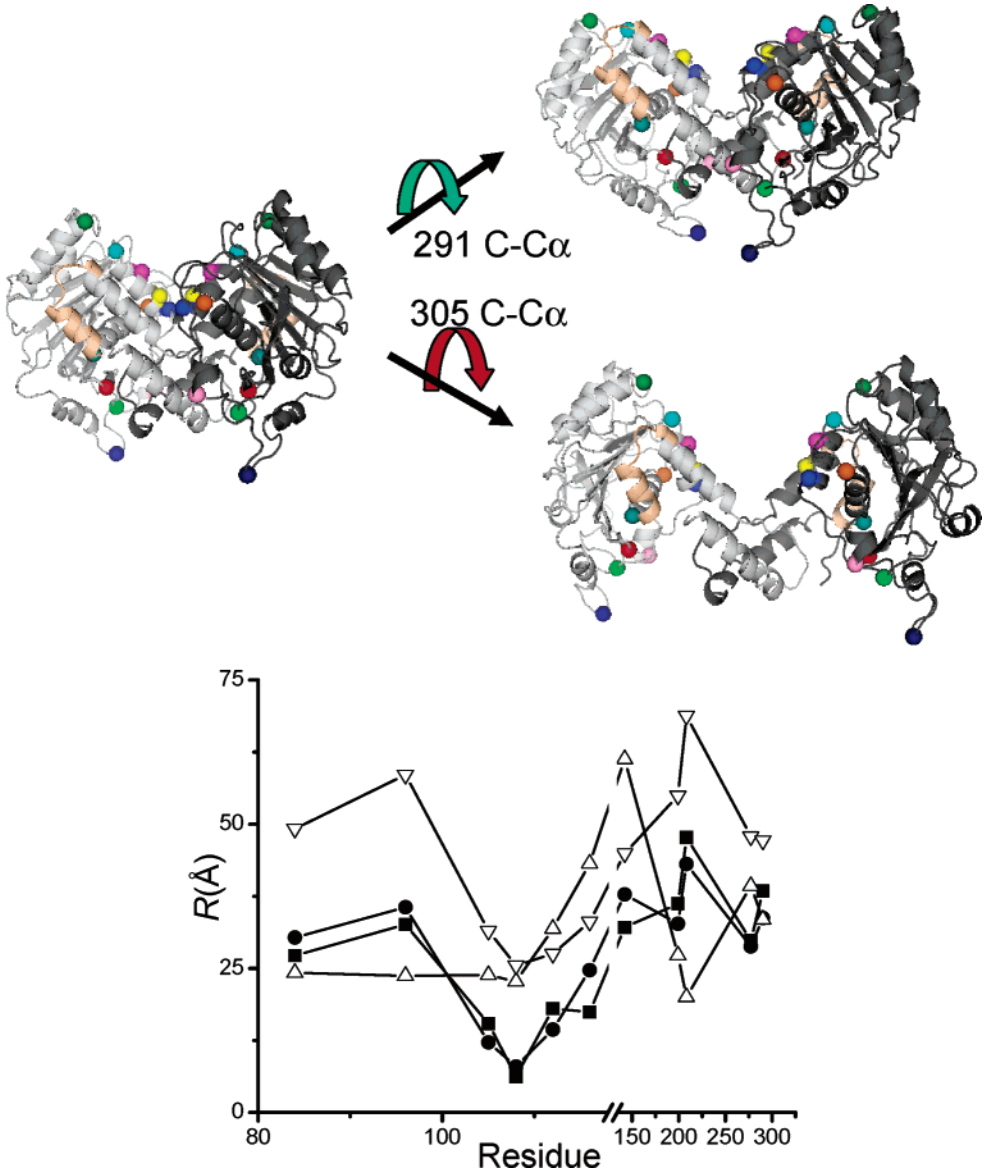

FIGURE 11: Comparison of interprobe distances for three structural models of cdb3. The ribbon structure on the left from the crystal structure shows 11 residues that were converted to the R1 side chain for interprobe distance measurements. The structure in the upper right was generated by a single 30° rotation about the C−C_α bond of Glu291. The structure in the lower right was generated by a single 30° rotation about the C−C_α bond of Gly305. The plot in the lower panel shows the experimentally determined interprobe distances at residues 84 (red), 96 (green), 105 (dark blue), 108 (yellow), 112 (purple), 116 (light blue), 142 (dark green), 199 (pink), 208 (blue), 277 (orange), and 290 (medium blue) as filled squares. The filled circles are the C_α−C_α distances from the crystal structure on the left. The open triangles are the C_α−C_α distances from the structural model in the upper right. The inverted open triangles are the C_α−C_α distances from the structural model in the lower right.

cdb3 were mutated to alanine and a unique cysteine was introduced at selected positions, spin labeled, and characterized using established approaches of site-directed spin labeling and EPR to elucidate secondary structure, tertiary structure contacts, solvent accessibility, and local side-chain dynamics (reviewed in refs *41*, *55*, *56*, *57*). Similarly, the quaternary structure of the cdb3 dimer was investigated using the recently developed pulsed EPR method, DEER. Collectively, the current studies have provided strong evidence that the structure of the central core of cdb3 at physiological pH is indistinguishable, within the limits of current resolution, from that reported for the crystal structure at pH 4.8. Additional studies have shown that the N- and C-termini of cdb3 are dynamically disordered.

Solid experimental evidence has shown that cdb3 undergoes reversible conformational rearrangements as a function of pH (e.g. tryptophan fluorescence (*19*), thermal stability (*16*), Stokes radius (*38*), and segmental dynamics (*39*)). However, the largest changes appear to occur in the pH range from 8 to 10, which is well outside the normal intracellular pH range of 7.2 to 7.4 for a human erythrocyte. Initial spin-labeling studies that have been carried out in the pH 8.5−10 range have yielded EPR spectral changes at these higher pH values (data not shown (*20*, *21*)). Future studies can be focused on analyzing these data to develop a structural model that may provide insights into the increased hydrodynamic radius, decreased thermal stability, increased dynamics, and decreased and shifted tryptophan fluorescence that have previously been reported. However, the most pressing question is: what is the structure of cdb3 under conditions that approximate the physiological environment within the erythrocyte? Therefore, the current work is focused on

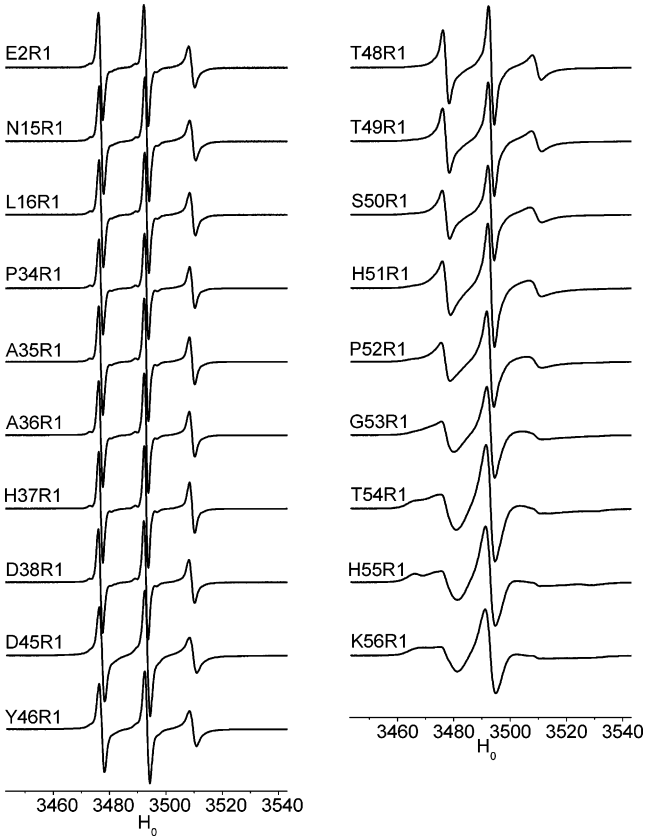

FIGURE 12: EPR characterization of the structure and dynamics of the N-terminus of cdb3. The conventional CW-EPR spectra at selected residues in the N-terminus of cdb3 are shown as 100 G displays normalized to the same amplitude.

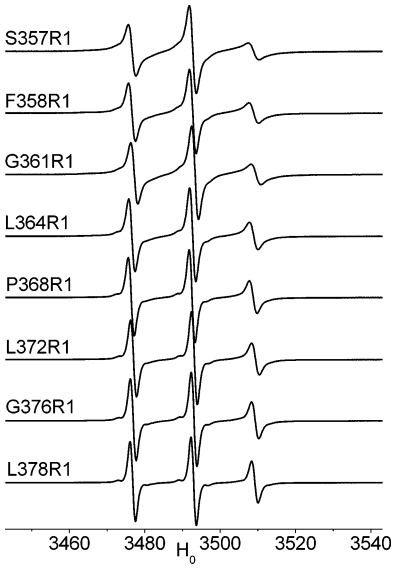

FIGURE 13: EPR characterization of the structure and dynamics of the C-terminus of cdb3. The conventional CW-EPR spectra at selected residues in the C-terminus of cdb3 are shown as 100 G displays normalized to the same amplitude.

answering the fundamental question of how the structure of cdb3 at neutral pH compares with the crystal structure determined from crystals grown at pH 4.8. It should be noted that it was not possible to compare EPR and DEER data from spin-labeled samples at neutral pH with the corresponding data obtained at pH 4.8 due to the tendency of many of the single cysteine mutants of cdb3 to aggregate at the lower pH. This aggregation, which was almost immediate for some samples, produced spectral shifts that masked any structural changes that might have occurred.

Structure of the Peripheral α^+ β*-Fold Domain.* The crystal structure of cdb3 showed that the peripheral protein binding domain was composed of a compact α^+ β-fold with the central β-sheet packed on both faces against α-helices. To assess the effect of pH on the global structure of the peripheral protein binding domain, residues 127−137, which comprise a major portion of the $\alpha 2^{128-141}$ surface exposed helix, were individually mutated to the R1 side chain and characterized by EPR as shown in Figures 4 and 5. The parametrized data in Figure 5 are consistent with an α-helix with one surface exposed to the water soluble paramagnetic broadening agent NiEDDA and the opposite face packed against the interior of the protein and inaccessible to NiEDDA. Likewise, the second moments of the EPR spectra, which provide a measure of the restriction of R1 side chain motion (e.g. ref *41*), are also consistent with residues 127−137 forming a standard α-helix. The data in Figure 5 (lower) are plotted as the inverse second moment so that the phase of the side chain mobility data is the same as the accessibility data (i.e. the least restricted R1 side chains with the largest inverse second moments have the highest exposure to water and the greatest accessibility to NiEDDA). The parametrized data in Figure 5 are all consistent with the structure and packing of this α-helix that was determined in the crystal structure. While these data do not rule out subtle structural rearrangements of the peripheral protein binding domain in solution at neutral pH, they do provide solid evidence that the local structure in, and around, the α2-helix is preserved. This observation, coupled with the compact globular nature of this domain with an extensive hydrophobic core, strongly suggests that the reported pH dependent conformational changes in cdb3 do not result from major changes in the structure of the peripheral protein binding domain in agreement with previous predictions (*3*).

Structure of the Dimer Interface in Cdb3. The crystal structure of cdb3 revealed extensive interactions, consisting of eight intermonomeric hydrogen bonds and a hydrophobic core of nine leucine residues, between the dimerization arms (residues 314−344) of each monomer (*3*). These multiple interactions, coupled with the fact that cdb3 is a stable dimer throughout the pH range where structural transitions have been observed, suggested that the local structure in the dimer interface was preserved at neutral pH. As a direct test of this tenet, residues 337 to 348 were individually converted to the R1 side chain and the EPR spectra characterized as shown in Figures 6 and 7. The parametrized data in Figure 7 show that these residues are contained in an α-helix (NiEDDA and inverse second moment show sinusoidal trends with an approximate periodicity of 3.6 residues) and the same surfaces of the helix are exposed to water and buried as reported in the crystal structure at pH 4.8 (*3*). These data provide solid indications that the local structure in, and around, helix 10 is the same at neutral pH as reported in the crystal structure.

The EPR spectrum at residue 339 (Q339R1; Figure 6) showed classic characteristics of a resolved intersubunit dipole−dipole interaction between the R1 side chains on adjacent monomers. Such highly resolved dipolar couplings are only seen in conventional continuous wave EPR spectra

when the two spin label probes are separated by 18 Å or less (see ref *43*) (*44*). Analysis of the EPR spectrum at this position, using a newly developed tether-in-a-cone model (*26*), yielded an interprobe distance of 14.7 Å (Figure 8). This is very close to the average predicted distance of 18.1 Å between the R1 side chains based on the static crystal structure and molecular modeling as shown in Figure 10.

The structure of the dimer interface was more fully characterized by DEER measurements at positions 340−345 as shown in Figure 9. The conventional EPR spectral shapes and line widths at each of these positions were characteristic of spatially isolated spin labels (Figure 6), indicating a separation of ≥25 Å (*27, 42−44*). However, as shown in Figure 9 and in Table 1, the interprobe distances were readily measured using DEER. As shown in Figure 10, the experimentally determined distances were in reasonable agreement with the average distances predicted from molecular modeling of allowed probe orientations. It is important to emphasize that the trend of measured intersubunit distances followed the $C_\alpha-C_\alpha$ distances calculated from the crystal structure throughout this region. The important points to be made in regard to the current work are that the experimental data in Figures 6 and 7 indicate that residues 337−348 are contained within a continuous α-helix and that the intersubunit (interhelical) distances between residues in the two helices in the cdb3 dimer (Figures 8−10) indicate that their spatial arrangement is the same, within the limits of current resolution, as reported in the crystal lattice. While it is not possible to absolutely rule out a subtle 1 to 2 Å rigid body change in helix position, it would be difficult to reconcile the entire body of experimental data in Figures 6, 7, 8, 9, and 10 with a larger change in position or relative orientation.

An important consideration in evaluating structural models that are derived or refined based on interprobe distance constraints obtained from conventional or pulsed EPR methods is how accurate these distances are. Accordingly, several studies have appropriately been devoted to making measurements on well-defined model systems using both continuous wave EPR (e.g. refs *27, 42, 58*) or pulsed EPR techniques including double quantum coherence (DQC (*47, 59*) and DEER (e.g. refs *33, 45*). Collectively, these studies have provided solid indications that average interprobe distances in the 8−50 Å range can be measured with accuracies on the order of ±2 Å when the distribution of distances is accurately taken into account. The greatest uncertainty remains how to accurately model the distribution of interprobe distances between the R1 side chains that reliably accounts for its inherent dimensions, flexibility, dynamics, and interactions as well as the dynamic contributions from backbone fluctuations or domain motions. Several recent studies have explored different ways of relating the experimentally determined average interprobe distances and distance distributions back to the local structure and dynamics of the protein including static modeling approaches (e.g. refs *47, 59*), combined Monte Carlo and molecular dynamics approaches (e.g. ref *48*), and pure molecular dynamics approaches (e.g. refs *46, 49, 60*). In the current work, the dimensions and accessible conformational space for the R1 side chain were modeled based on the local environment in the static crystal structure. Molecular dynamics simulations (not shown) were also explored in these studies and found to give reasonable results for buried, motionally constrained sites (e.g. residues 339, 342, and 343) but much less realistic sampling at surface exposed sites (e.g. sites 344 and 345) where short (2 ns) simulations in a vacuum greatly underestimated the distribution of distances recovered from fitting the DEER data and the apparent accessible space from the crystal structure. More extensive molecular dynamics simulations including longer trajectories using both continuum and explicit solvent models, which are currently being pursued, may eventually prove to be an effective method for characterizing the conformational space of the R1 side chain including the effects of local backbone fluctuations. Further development of robust methods for relating the average distances and the distribution of distances for interactions between R1 side chains remains an active area of investigation in site-directed spin labeling.

Current efforts are also being directed toward improving the methods for recovering the true distribution of distances from experimental DEER and DQC data (e.g. refs *61−63*). The implementation of these newer methods, along with obtaining experimental data at a variety of microwave frequencies, should provide the capability to more rigorously evaluate more complex distance distribution models (e.g. bimodal or multimodal) in future work.

Quaternary Structure of the Cdb3 Dimer at Neutral pH. Based upon the crystal structure at pH 4.8, it was hypothesized that the pH dependent changes in cdb3 that had been reported in the literature did not involve changes in the peripheral protein binding domain nor in the dimer interface but that it might involve changes in the positioning of these two domains relative to each other (*3*). Specifically, plausible models for the expansion or elongation of the cdb3 dimer could be generated by single rotations about glutamic acid 291, located between helices α7 and α8, or about glycine 305, located between helices α8 and α9. The resulting families of structures could be generated without any significant changes in the secondary structure of the cdb3 dimer. Figure 11 shows two elongated structures that were generated either by a 30° rotation about the $C-C_\alpha$ bond of Glu291 (upper right) or by a 30° rotation about the $C-C_\alpha$ bond of Gly305 (lower right). The graphical data show that experimental intersubunit distance measurements agree very well with the $C_\alpha-C_\alpha$ distances calculated from the crystal structure (rms deviation of 4.1 Å) but do not agree in magnitude or trend with the $C_\alpha-C_\alpha$ distances calculated from the model generated by rotation about Glu 291 (rms deviation of 16.8 Å) or by rotation about Gly305 (rms deviation of 17.6 Å). Given the excellent agreement in overall trend of distances and the extensive coverage of labeling, it is reasonable to conclude that the tertiary structure of the cdb3 dimer at neutral pH is remarkably similar to the structure reported in the crystal lattice at pH 4.8.

This conclusion is compatible with a recent study that utilized luminescence resonance energy transfer to measure the distance between Cys201 residues on adjacent monomers of the isolated cdb3 dimer (*64*). Specifically, this study reported a small 2 Å change in interprobe separation between pH 5 and 8 and a large 8 Å change between pH 8 and 10. The small 2 Å change between pH 5 and 8, which might be due in part to the breaking of a hydrogen bond between aspartic acid 316 (Asp316) and tryptophan 105 (Trp105) as previously hypothesized (*3*), cannot be ruled out based on the current data. Interestingly, this study did report an 8 Å

change in interprobe separation between pH 5 and 8 when measurements were carried out on full length AE1 in KI-stripped inside out vesicles prepared from erythrocyte membranes. This interesting preliminary observation, which could indicate that the pH dependent structural transitions of the cytoplasmic domain are quite different in full length AE1, merits further investigation once high level expression and purification of the full length protein is accomplished.

Another possibility that should be considered is whether cdb3 adopts the same structure in the crystal lattice from crystals grown at pH 4.8 as it does in solution at pH 4.8. It is entirely possible that crystal packing forces could select for a conformation of cdb3 that is similar, or the same, as its conformation in solution at neutral pH. Along these lines, it is interesting to note that there was some asymmetry between the two monomers in the crystal structure and that the N- and C-termini were resolved to different residues in the two monomers in the crystal lattice. Examination of the crystal lattice suggests that these differences may be due to crystal packing interactions. This idea is supported by the current EPR data which do not give any indications (e.g. two-component spectra or unusual spectral broadening) of differences in dynamics or ordering of the two N- or two C-termini in the cdb3 dimer in those regions near the boundary of resolved residues in the crystal structure, suggesting that the asymmetry observed in the crystal structure does not exist in solution.

Structure and Dynamics of the N- and C−Termini of Cdb3. The N- and C-termini of cdb3 both play important roles in the human erythrocyte with the N-terminus serving as a site for binding of several intracellular proteins (reviewed in ref *1*) and the C-terminus providing a physical link between the membrane skeleton−ankyrin−cdb3 complex and the transmembrane domain of AE1. Though previous work had provided indications that the N-terminus of cdb3 binds aldolase (*65*) and hemoglobin (*13*) in an extended conformation, and it would be difficult to bind these peripheral proteins to a compact and highly structured N-terminus without steric interference from the lipid bilayer (*3*), little direct evidence for its structure has been reported. The data in Figure 12 provide compelling evidence that the entire N-terminus lacks stable secondary structure and that it is highly dynamic on the EPR (nanosecond) time scale. Using an average value of 3.5 Å for the length of a single amino acid, the N-terminal methionine of cdb3 (residues 1−54) could be located 189 Å away from the point of entry into the structured central core in its fully extended conformation. The ability of the N-terminus to exist in such an extended conformation could explain how the highly acidic distal region can bind to a wide range of rather large intracellular proteins without interference from the cytoplasmic surface of the bilayer.

It is possible that the highly acidic N-terminus could interact with the globular core of cdb3 in a pH dependent manner. Changes in the nature and extent of such interactions could contribute, in part, to the observed changes in intrinsic tryptophan fluorescence and to the increase in radius of the protein at higher pH. Additional studies will be required to test these possibilities.

Several lines of experimental evidence have suggested that at least a portion of the C-terminal segment of cdb3 is flexible and possibly lacks secondary structure (*50*, *66*, *67*; reviewed in ref *53*). The data in Figure 13 show that, in the isolated cdb3 dimer, residues 357−378 are indeed dynamic on the nanosecond time scale and lacking in stable secondary structure. While these data do not prove that this region is likewise unstructured in full length AE1, they are consistent with many experimental observations in the full length protein including the high degree of susceptibility to proteolysis at residue 379 (*66*), the limited restriction of rotational motion of the transmembrane domain of that subpopulation of AE1 that is bound to the membrane skeleton via ankyrin (*50*, *67*), and the structural and functional independence of the two domains.

Conclusions. The body of site-directed spin labeling data reported in this work indicates that the solution structure of the central core of cdb3 at neutral pH is remarkably similar to the structure previously reported from crystals grown at pH 4.8. While the resolution currently available from these EPR studies is not sufficient to rule out small structural differences, it is significant that the entire body of data obtained from 34 different sites in the central core domain is remarkably consistent with the static crystal structure. The results further suggest that the structural changes that have been detected in the pH 5 to 8 range using techniques such as intrinsic tryptophan fluorescence are likely due to localized changes and not to large global changes in the structure of cdb3. The N- and C-termini are very dynamic on the nanosecond time scale and do not exhibit detectable regions of stable secondary structure. These latter observations explain a number of previous observations including the ability of the N-terminus to bind relatively large intracellular proteins and the limited motional coupling between the cytoplasmic and transmembrane domains of full length AE1.

ACKNOWLEDGMENT

The authors thank Dr. Hassane Mchaourab for critiquing the manuscript prior to submission and for many helpful discussions during the course of the work. Drs. Piotr Fajer and Jurek Krzystek are gratefully acknowledged for providing assistance in obtaining DEER data at the National High Magnetic Field Laboratory. The Vanderbilt Center for Structural Biology provided access to instrumentation as well as technical support from Dr. Laura Mizoue for making CD and DSC measurements.

REFERENCES

1. Low, P. S. (1986) Structure and function of the cytoplasmic domain of band 3: center of erythrocyte membrane-peripheral protein interactions, *Biochim. Biophys. Acta 864*, 145−167.
2. Tanner, M. J. (1997) The structure and function of band 3 (AE1): recent developments (review), *Mol. Membr. Biol. 14*, 155−165.
3. Zhang, D., Kiyatkin, A., Bolin, J. T., and Low, P. S. (2000) Crystallographic structure and functional interpretation of the cytoplasmic domain of erythrocyte membrane band 3, *Blood 96*, 2925−2933.
4. Bennett, V., and Stenbuck, P. J. (1980) Association between ankyrin and the cytoplasmic domain of band 3 isolated from the human erythrocyte membrane, *J. Biol. Chem. 255*, 6424−6432.
5. Korsgren, C., and Cohen, C. M. (1986) Purification and properties of human erythrocyte band 4.2. Association with the cytoplasmic domain of band 3, *J. Biol. Chem. 261*, 5536−5543.
6. Pasternack, G. R., Anderson, R. A., Leto, T. L., and Marchesi, V. T. (1985) Interactions between protein 4.1 and band 3. An alternative binding site for an element of the membrane skeleton, *J. Biol. Chem. 260*, 3676−3683.
7. Kant, J. A., and Steck, T. L. (1973) Specificity in the association of glyceraldehyde 3-phosphate dehydrogenase with isolated human erythrocyte membranes, *J. Biol. Chem. 248*, 8457−8464.

8. Strapazon, E., and Steck, T. L. (1976) Binding of rabbit muscle aldolase to band 3, the predominant polypeptide of the human erythrocyte membrane, *Biochemistry 15*, 1421−1424.
9. Karadsheh, N. S., and Uyeda, K. (1977) Changes in allosteric properties of phosphofructokinase bound to erythrocyte membranes, *J. Biol. Chem. 252*, 7418−7420.
10. Beth, A. H., Balasubramanian, K., Wilder, R. T., Venkataramu, S. D., Robinson, B. H., Dalton, L. R., Pearson, D. E., and Park, J. H. (1981) Structural and motional changes in glyceraldehyde-3-phosphate dehydrogenase upon binding to the band-3 protein of the erythrocyte membrane examined with [15N,2H]maleimide spin label and electron paramagnetic resonance, *Proc. Natl. Acad. Sci. U.S.A. 78*, 4955−4959.
11. Shaklai, N., Yguerabide, J., and Ranney, H. M. (1977) Interaction of hemoglobin with red blood cell membranes as shown by a fluorescent chromophore, *Biochemistry 16*, 5585−5592.
12. Salhany, J. M., and Shaklai, N. (1979) Functional properties of human hemoglobin bound to the erythrocyte membrane, *Biochemistry 18*, 893−899.
13. Walder, J. A., Chatterjee, R., Steck, T. L., Low, P. S., Musso, G. F., Kaiser, E. T., Rogers, P. H., and Arnone, A. (1984) The interaction of hemoglobin with the cytoplasmic domain of band 3 of the human erythrocyte membrane, *J. Biol. Chem. 259*, 10238−10246.
14. Waugh, S. M., and Low, P. S. (1985) Hemichrome binding to band 3: nucleation of Heinz bodies on the erythrocyte membrane, *Biochemistry 24*, 34−39.
15. Harrison, M. L., Isaacson, C. C., Burg, D. L., Geahlen, R. L., and Low, P. S. (1994) Phosphorylation of human erythrocyte band 3 by endogenous p72syk, *J. Biol. Chem. 269*, 955−959.
16. Appell, K. C., and Low, P. S. (1981) Partial structural characterization of the cytoplasmic domain of the erythrocyte membrane protein, band 3, *J. Biol. Chem. 256*, 11104−11111.
17. Colfen, H., Harding, S. E., Boulter, J. M., and Watts, A. (1996) Hydrodynamic examination of the dimeric cytoplasmic domain of the human erythrocyte anion transporter, band 3, *Biophys. J. 71*, 1611−1615.
18. Weinstein, R. S., Khodadad, J. K., and Steck, T. L. (1978) Fine structure of the band 3 protein in human red cell membranes: freeze-fracture studies, *J. Supramol. Struct. 8*, 325−335.
19. Zhou, J., and Low, P. S. (2001) Characterization of the reversible conformational equilibrium in the cytoplasmic domain of human erythrocyte membrane band 3, *J. Biol. Chem. 276*, 38147−38151.
20. Cobb, C. E., Dixit, M., Brandon, S., Hustedt, E. J., and Beth, A. H. (2003) Investigation of pH-induced structural changes of cdb3 by site-directed spin labeling, *Biophys. J. 84*, 496a (abstract).
21. Cobb, C. E., Silvestry, M., Zhou, Z., Camarata, A., Dixit, M., Brandon, S., Hustedt, E. J., and Beth, A. H. (2004) Investigation of the structure and stability of cdb3 by site-directed spin labeling and intrinsic tryptophan fluorescence, *Biophys. J. 86*, 100a (abstract).
22. Zhou, Z., Desensi, S., Brandon, S., Dixit, N., Cobb, C. E., Hustedt, E. J., and Beth, A. H. (2005) Solution structure of cdb3 from site directed spin labeling studies and double electron-electron resonance, *Biophys. J. 88*, 265a (abstract).
23. Studier, F. W. (2005) Protein production by auto-induction in high-density shaking cultures, *Protein Expression Purif. 41*, 207−234.
24. Laemmli, U. K. (1970) Cleavage of structural proteins during the assembly of the head of bacteriophage T4, *Nature 227*, 680−685.
25. Slichter, C. P. (1980), in *Principles of Magnetic Resonance*, M. Cardona, P. Fulde, and H.-J. Queisser, Eds., p 69, Springer-Verlag, Berlin, Heidelberg, New York.
26. Hustedt, E. J., Stein, R. A., Sethaphong, L., Brandon, S., Zhou, Z., and DeSensi, S. C. (2005) Dipolar coupling between nitroxide spin labels: the development of a tether in a cone model, *Biophys. J.* (in press).
27. Rabenstein, M. D., and Shin, Y. K. (1995) Determination of the distance between two spin labels attached to a macromolecule, *Proc. Natl. Acad. Sci. U.S.A. 92*, 8239−8243.
28. Steinhoff, H. J., Radzwill, N., Thevis, W., Lenz, V., Brandenburg, D., Antson, A., Dodson, G., and Wollmer, A. (1997) Determination of interspin distances between spin labels attached to insulin: comparison of electron paramagnetic resonance data with the X-ray structure, *Biophys. J. 73*, 3287−3298.
29. Subczynski, W. K., and Hyde, J. S. (1981) The diffusion-concentration product of oxygen in lipid bilayers using the spin-label T1 method, *Biochim. Biophys. Acta 643*, 283−291.
30. Altenbach, C., Flitsch, S. L., Khorana, H. G., and Hubbell, W. L. (1989) Structural studies on transmembrane proteins. 2. Spin labeling of bacteriorhodopsin mutants at unique cysteines, *Biochemistry 28*, 7806−7812.
31. Pannier, M., Veit, S., Godt, A., Jeschke, G., and Spiess, H. W. (2000) Dead-time free measurement of dipole-dipole interactions between electron spins, *J. Magn. Reson. 142*, 331−340.
32. Jeschke, G. (2002) Determination of the nanostructure of polymer materials by electron paramagnetic resonance spectroscopy, *Macromol. Rapid Commun. 23*, 227−246.
33. Jeschke, G. (2002) Distance measurements in the nanometer range by pulse EPR, *ChemPhysChem 3*, 927−932.
34. Jeschke, G., Koch, A., Jonas, U., and Godt, A. (2002) Direct conversion of EPR dipolar time evolution data to distance distributions, *J. Magn. Reson. 155*, 72−82.
35. Langen, R., Oh, K. J., Cascio, D., and Hubbell, W. L. (2000) Crystal structures of spin labeled T4 lysozyme mutants: implications for the interpretation of EPR spectra in terms of structure, *Biochemistry 39*, 8396−8405.
36. Columbus, L., Kalai, T., Jeko, J., Hideg, K., and Hubbell, W. L. (2001) Molecular motion of spin labeled side chains in alpha-helices: analysis by variation of side chain structure, *Biochemistry 40*, 3828−3846.
37. Macke, T., and Case, D. A. (1998) Modeling unusual nucleic acid structures, in *Molecular Modeling of Nucleic Acids*, pp 379−393, American Chemical Society, Washington, DC.
38. Low, P. S., Westfall, M. A., Allen, D. P., and Appell, K. C. (1984) Characterization of the reversible conformational equilibrium of the cytoplasmic domain of erythrocyte membrane band 3, *J. Biol. Chem. 259*, 13070−13076.
39. Thevenin, B. J., Periasamy, N., Shohet, S. B., and Verkman, A. S. (1994) Segmental dynamics of the cytoplasmic domain of erythrocyte band 3 determined by time-resolved fluorescence anisotropy: sensitivity to pH and ligand binding, *Proc. Natl. Acad. Sci. U.S.A. 91*, 1741−1745.
40. Farahbakhsh, Z. T., Altenbach, C., and Hubbell, W. L. (1992) Spin labeled cysteines as sensors for protein−lipid interaction and conformation in rhodopsin, *Photochem. Photobiol. 56*, 1019−1033.
41. Hubbell, W. L., McHaourab, H. S., Altenbach, C., and Lietzow, M. A. (1996) Watching proteins move using site-directed spin labeling, *Structure 4*, 779−783.
42. Hustedt, E. J., Smirnov, A. I., Laub, C. F., Cobb, C. E., and Beth, A. H. (1997) Molecular distances from dipolar coupled spin-labels: the global analysis of multifrequency continuous wave electron paramagnetic resonance data, *Biophys. J. 72*, 1861−1877.
43. Hustedt, E. J., and Beth, A. H. (1999) Nitroxide spin-spin interactions: applications to protein structure and dynamics, *Annu. Rev. Biophys. Biomol. Struct. 28*, 129−153.
44. Hustedt, E. J., and Beth, A. H. (2000) Structural information from cw-EPR spectra of dipolar coupled nitroxide spin labels, in *Biological Magnetic Resonance, 19: Distance Measurements in Biological Systems by EPR* (Berliner, L. J., Eaton, S. S., and Eaton, G. R., Eds.), pp 155−184, Kluwer Academic/Plenum Publishers, New York.
45. Jeschke, G., Pannier, M., and Spiess, H. W. (2000) Double electron-electron resonance, in *Biological Magnetic* Resonance, *19: Distance Measurements in Biological Systems by EPR* (Berliner, L. J., Eaton, S. S., and Eaton, G. R., Eds.), pp 493−512, Kluwer Academic/Plenum Publishers, New York.
46. Poirier, M. A., Xiao, W., Macosko, J. C., Chan, C., Shin, Y. K., and Bennett, M. K. (1998) The synaptic SNARE complex is a parallel four-stranded helical bundle, *Nat. Struct. Biol. 5*, 765−769.
47. Borbat, P. P., McHaourab, H. S., and Freed, J. H. (2002) Protein structure determination using long-distance constraints from double-quantum coherence ESR: study of T4 lysozyme, *J. Am. Chem. Soc. 124*, 5304−5314.
48. Sale, K., Sar, C., Sharp, K. A., Hideg, K., and Fajer, P. G. (2002) Structural determination of spin label immobilization and orientation: a Monte Carlo minimization approach, *J. Magn. Reson. 156*, 104−112.
49. Schiemann, O., Piton, N., Mu, Y., Stock, G., Engels, J. W., and Prisner, T. F. (2004) A PELDOR-based nanometer distance ruler for oligonucleotides, *J. Am. Chem. Soc. 126*, 5722−5729.
50. Blackman, S. M., Hustedt, E. J., Cobb, C. E., and Beth, A. H. (2001) Flexibility of the cytoplasmic domain of the anion exchange protein, band 3, in human erythrocytes, *Biophys. J. 81*, 3363−3376.

51. Moriyama, R., Ideguchi, H., Lombardo, C. R., Van Dort, H. M., and Low, P. S. (1992) Structural and functional characterization of band 3 from Southeast Asian ovalocytes, *J. Biol. Chem. 267*, 25792−25797.
52. Schofield, A. E., Tanner, M. J., Pinder, J. C., Clough, B., Bayley, P. M., Nash, G. B., Dluzewski, A. R., Reardon, D. M., Cox, T. M., and Wilson, R. J. (1992) Basis of unique red cell membrane properties in hereditary ovalocytosis, *J. Mol. Biol. 223*, 949−958.
53. Wang, D. N. (1994) Band 3 protein: structure, flexibility and function, *FEBS Lett. 346*, 26−31.
54. Michaely, P., Tomchick, D. R., Machius, M., and Anderson, R. G. (2002) Crystal structure of a 12 ANK repeat stack from human ankyrinR, *EMBO J. 21*, 6387−6396.
55. Hubbell, W. L., and Altenbach, C. (1994) Investigation of structure and dynamics in membrane proteins using site-directed spin labeling, *Curr. Opin. Struct. Biol. 4*, 566−573.
56. Hubbell, W. L., Gross, A., Langen, R., and Lietzow, M. A. (1998) Recent advances in site-directed spin labeling of proteins, *Curr. Opin. Struct. Biol. 8*, 649−656.
57. Feix, J. B., and Klug, C. S. (1998) Site-directed spin labeling of membrane proteins and membrane interactions, in *Biological Magnetic Resonance, 14*: *Spin Labeling: The Next Millenium* (Berliner, L. J., Ed.) pp 251−281, Plenum Press, New York.
58. Kim, N. K., Murali, A., and DeRose, V. J. (2004) A distance ruler for RNA using EPR and site-directed spin labeling, *Chem. Biol. 11*, 939−948.
59. Borbat, P. P., Davis, J. H., Butcher, S. E., and Freed, J. H. (2004) Measurement of large distances in biomolecules using double-quantum filtered refocused electron spin-echoes, *J. Am. Chem. Soc. 126*, 7746−7747.
60. Fu, Z., Aronoff-Spencer, E., Backer, J. M., and Gerfen, G. J. (2003) The structure of the inter-SH2 domain of class IA phosphoinositide 3-kinase determined by site-directed spin labeling EPR and homology modeling, *Proc. Natl. Acad. Sci. U.S.A. 100*, 3275−3280.
61. Jeschke, G., Panek, G., Godt, A., Bender, A., and Paulsen, H. (2004) Data analysis procedures for pulse ELDOR measurements of broad distance distributions, *Appl. Magn. Reson. 26*, 223−244.
62. Chiang, Y. W., Borbat, P. P., and Freed, J. H. (2005) The determination of pair distance distributions by pulsed ESR using Tikhonov regularization, *J. Magn. Reson. 172*, 279−295.
63. Bowman, M. K., Maryasov, A. G., Kim, N., and DeRose, V. J. (2004) Visualization of distance distribution from pulsed double electron-electron resonance data, *Appl. Magn. Reson. 26*, 23−39.
64. Pal, P., Holmberg, B., Lesiione, J., and Knauf, P. A. (2005) Effects of pH and peripheral protein binding on the structure of the cytoplasmic domain of AE1 observed by resonance energy transfer, *Biophys. J. 88*, 47a (abstract).
65. Schneider, M. L., and Post, C. B. (1995) Solution structure of a band 3 peptide inhibitor bound to aldolase: a proposed mechanism for regulating binding by tyrosine phosphorylation, *Biochemistry 34*, 16574−16584.
66. Steck, T. L., Ramos, B., and Strapazon, E. (1976) Proteolytic dissection of band 3, the predominant transmembrane polypeptide of the human erythrocyte membrane, *Biochemistry 15*, 1153−1161.
67. Nigg, E. A., and Cherry, R. J. (1980) Anchorage of a band 3 population at the erythrocyte cytoplasmic membrane surface: protein rotational diffusion measurements, *Proc. Natl. Acad. Sci. U.S.A. 77*, 4702−4706.
68. Hustedt, E. J., Cobb, C. E., Beth, A. H., and Beechem, J. M. (1993) Measurement of rotational dynamics by the simultaneous nonlinear analysis of optical and EPR data, *Biophys. J. 64*, 614−621.

BI050931T